

Research Article

Experimental and Numerical Studies on Flowing Properties of Grouting Mortar Based on the Modified MPS Method

Ailifeila Aierken ^{1,2}, Shilin Luo ^{1,3}, Jianqing Jiang ¹, Linlin Chong ^{1,2}, Jin Chang ¹,
Rui Zhang ¹ and Xiangchao Zhang ^{1,2}

¹College of Civil Engineering, Changsha University, Changsha 410022, China

²Innovation Center for Environmental Ecological and Green Building Materials of CCSU, Changsha University, Changsha 410022, China

³College of Civil Engineering and Geomatics, Chang'an University, Xi'an 710064, China

Correspondence should be addressed to Shilin Luo; rosilynn@cqu.edu.cn

Received 16 April 2022; Accepted 2 June 2022; Published 22 June 2022

Academic Editor: Zizheng Guo

Copyright © 2022 Ailifeila Aierken et al. This is an open access article distributed under the Creative Commons Attribution License, which permits unrestricted use, distribution, and reproduction in any medium, provided the original work is properly cited.

Grouting mortar has widespread application in engineering because of the advantages of good durability, low cost, and environmental friendliness. To study the flowing properties of grouting mortar, laboratory minislump tests taking different rheological parameters of grouting mortar into consideration were conducted to obtain the flow time and flow pattern of grouting mortar. A modified MPS method (moving-particle semi-implicit method) introduced two sections of Bingham rheological, and segregation was proposed. The effects of the plastic viscosity on the flow state of mortar were studied, and the relationship between the plastic viscosity and the flowing time was established. The numerical results show that the modified MPS method can be used to predict the flow time and flow pattern of mortar in the template, and plastic viscosity has a great influence on the flow time of concrete, and with the increase of plastic viscosity, the time to flow to the specified area also increases. Moreover, the analysis of the rheological parameters can provide the basis for the design of mix ratio in the construction practice.

1. Introduction

In a variety of seismic reinforcement methods for concrete structures, the steel plate lining method is widely used to reinforce existing bridge piers or columns. In this method, the properties of grouting materials must be carefully controlled to fill the narrow gap between the steel plate and the structure. Otherwise, the reinforcement will not perform the expected strength in the design. Among the properties of grouting materials, fluidity and segregation-resistance are the most important properties to control the filling process.

From a computational point of view, choosing the right strategy for the simulation is an important issue, and several approaches have been tried to simulate the flow of these approaches in previous studies [1–3]. The

CFD software is usually employed to simulate the pipe flow to predict the velocity distribution and pressure loss. However, fresh concrete is considered a single-phase fluid in CFD methods, it is unable to provide information about the dynamic segregation of concrete in the pipe for predicting blockage [4–6]. Recently, the meshless particle method, such as Smoothed Particle Hydrodynamics (SPH) method [7], has been increasingly used in the flow simulation of fluid, which represents the fluid with particles. The meshless particle method has the potential to numerically discuss aggregate segregation [8]. The SPH method has been proved to be applied to the flow simulation of fresh concrete [9–12]. There is no doubt that accurate calculation of pressure is important for the grouting mortar simulation. However, since the magnitude of the time step is limited in the SPH, the accuracy and efficiency

of calculation are greatly reduced. For analyzing the incompressible fluid problem, Koshizuka and Oka [13] developed a new meshless method named moving-particle semi-implicit method (MPS). The MPS has been successfully used in the simulation of multiphase flows under high pressure [14], and the flow simulations of fresh cementitious fluid [15, 16], and has special advantages in simulating flow and filling behavior. Li et al. [17] and Jing-jun et al. [18] used the MPS method to simulate the flow characteristics of SCC and RFC in the L-box test. The results show that this method can simulate the flow process of SCC in rock-filled bodies, predict the compactness of RFC, and ultimately provide a reference for the design and construction practice of RFC engineering [19–21]. The MPS method was also used to investigate the geohazard mechanism [22, 23] and flow performances of concrete [24, 25]. Thus, the numerical simulation method including MPS has been widely used in many geotechnical applications, such as mining engineering, tunnel engineering, and slope engineering [26–32].

This paper was aimed at extending the MPS approach to simulate the flow of grouting mortar in a minislump test. This methodology provided a thorough understanding of whether a minislump test can satisfy the self-compatibility criterion of passing ability through narrow gaps beside the flowability criterion. The result is compared with the flow time and flow pattern of the minislump test in the laboratory. By using this method, the effects of the plastic viscosity on the flow state of mortar in the minislump test are studied. The relationship between the plastic viscosity, the flowing time, and the density of mortar which is calculated as the ratio of mass to volume of the test is established. On this basis, the material segregation constitutive model is proposed. The distribution of aggregates in the mixes will also be tracked during the simulation to check whether or not they are homogeneously distributed after the flow has stopped. Simultaneously, it can provide a reference basis for the design and construction practice of cement mortar in engineering.

2. Methodology

2.1. Experimental Method

2.1.1. Material Preparation. In this study, grouting mortar was chosen as a grouting material and used minislump test to measure the flow properties. Three kinds of mix proportions of grouting mortar were presented according to the rational mix design method proposed in [19, 20]. All of the mix designation, cement, water, fine aggregate, and natural river sand among these three schemes were unchanged, which is 0.4, 969, 388, 621, and 156, respectively. The variations of rheological parameters of grouting mortar were changeable and controlled by different mix proportions of thickening agent and polycarboxylate superplasticizer. The detailed compositions of all mixes were given in Table 1. It should be noted that only W/C ratio of 0.4 was selected in this paper because we want to test the feasibility of the modified MPS method. Next step, we will try to simulate the flow

TABLE 1: Mix proportion of grouting mortar, kg/m³.

No	Mix designation	Cement	Water	FA ^a		VMAS ^b (W × %)	HRWR ^c (C × %)
				FA*	FA**		
1						0.0	0.9
2	0.4	969	388	621	156	0.45	2.0
3						0.1	0.7

^aFine aggregate <2.5 mm (note: a part of the fine aggregate is the coarser fraction of the limestone powder, FA* 125 μm–1.2 mm, whereas FA** refers to natural river sand ≥1.2 mm). ^bThickening agent. ^cPolycarboxylate superplasticizer.

pattern of mortar and concrete under different mix proportions.

2.1.2. Testing Apparatus. The minislump flow test is widely used in laboratories and construction sites for detecting grouting mortar flow characteristics. In this work, the slump cylinder was placed on the wet plate, and the mortar was injected into the cylinder, size, and shape of the cylinder as shown in Figure 1. The linear scraper was used to smooth the upper surface of the mortar, and sector scraper was adapted to remove the residual mortar dripping on the glass plate. Dampen the cylinder mold and place it on a flat moist glass plate, fill the mold with mortar, and remove the mold immediately by raising it in a vertical direction after striking off the surface by screeding. Measure the time when the mortar reach 250 mm, the diameter of the two right angles was measured with a ruler, and the average value was obtained as the flow value. The volume of the mix in the mold is 1.96×10^5 mm³ with a diameter and height of 50 mm and 100 mm, respectively.

2.2. Modified MPS Method. The accurate prediction of the mortar flowing behavior is not a simple task, particularly in the presence of a complex formwork shape. In this regard, the indispensable and inexpensive approach offering considerable potential is the numerical simulation of grouting mortar. MPS method applies a prediction–correction semi-implicit computation algorithm, which calculates external force and viscous term in the prediction step and calculates pressure term in the correction step. Since the MPS method has been brought forward for only two decades, it is considered one promising but immature method. Some drawbacks still exist with the MPS method, particularly in the investigation of the flowing properties of grouting mortar with different viscosity coefficients. Thus, a modified MPS method introduced two sections of Bingham rheological and segregation was developed. Actually, through the comparison between the numerical simulation and the experimental results by using modified MPS method, it is found that the simulation accuracy was improved. Simultaneously, it can provide a reference basis for the design and construction practice of cement mortar in engineering.

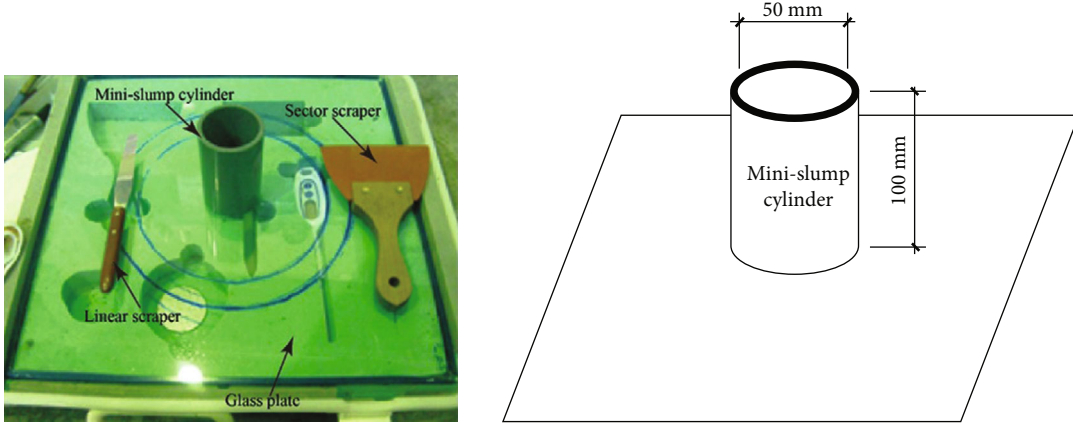


FIGURE 1: Size and shape of the minislump test.

2.2.1. *Governing Equations.* The governing equations for incompressible viscous flows are the mass conservation and Navier-Stokes equations:

$$\frac{D\rho}{Dt} = 0, \quad (1)$$

$$\frac{D\mathbf{u}}{Dt} = -\frac{1}{\rho}\nabla P + \nu\nabla^2\mathbf{u} + \mathbf{g}, \quad (2)$$

where ρ is the density, t is the time, \mathbf{u} is the velocity vector, P is the pressure, ν is dynamic viscosity, and \mathbf{g} is the acceleration due to gravity.

In the MPS method, the density and pressure increase when particles come close to each other and vice versa. The interaction between particles uses the weight function:

$$w(r_{ij}) \begin{cases} \frac{r_e}{r_{ij}} - 1 & (0 < r_{ij} < r_e), \\ 0 & (r_e \leq r_{ij}), \end{cases} \quad \text{Otherwise,} \quad (3)$$

where r_{ij} is the distance between particle i and j , and r_e is the effective radius. r_e is chosen as $2.1r_{ij}$ [13]. All the forms of the weight function satisfy that the weight values are non-zero in the region of effective radius and the weight function increases as r_{ij} decreases and vice versa. It means that the r_{ij} will increase when the distance between particles is closer than r_e and becomes zero when the distance is farther than r_e .

The particle number density, which is proportional to the mass density, at the position of the particle i is defined as

$$n_i = \sum_{j \neq i} w(|r_j - r_i|), \quad (4)$$

where r_i and r_j are the position vector of the i th and j th particles, respectively, and n_i is the particle number density of the i th particle.

The discretization models of MPS method are derived from the Taylor expansion, and the gradient and Laplacian

models in the MPS method are given as

$$\begin{aligned} \langle \nabla \varnothing \rangle_i &= \frac{d}{n^0} \sum_{j \neq i} \left[\left(\frac{(\varnothing_j - \varnothing_i)}{|\vec{r}_j - \vec{r}_i|^2} |\vec{r}_j - \vec{r}_i| \right) w(|\vec{r}_j - \vec{r}_i|) \right], \\ \langle \nabla^2 \varnothing \rangle_i &= \frac{2d}{\lambda n^0} \sum_{j \neq i} (\varnothing_j - \varnothing_i) w(|\vec{r}_j - \vec{r}_i|), \end{aligned} \quad (5)$$

where \varnothing_j and \varnothing_i are the quantities possessed by particles i and j , respectively, n^0 is the constant particle number density, d is the number of spatial dimensions, and λ is the Laplacian model coefficient, which is defined as

$$\lambda = \frac{\sum_{j \neq i} \mathbf{w}(|r_j - r_i|) |r_j - r_i|^2}{\sum_{j \neq i} \mathbf{w}(|r_j - r_i|)}. \quad (6)$$

This parameter adjusts the increase in the variance caused by the Laplacian model to that of the analytical solution. The gradient and Laplacian models are substituted into their corresponding operators in Equation (2). and the pressure, velocity, and position can be obtained. Substitute the velocity and pressure of each particle into the Lagrangian model. The source term of pressure can be represented by

$$\langle \nabla^2 P \rangle_i = \frac{2d}{\lambda n^0} \sum_{j \neq i} [(P_j - P_i) w(|r_j - r_i|)], \quad (7)$$

where P_j and P_i is the pressure of the i th and j th fluid particles, respectively. Substitute the pressure of particles into the gradient model. The pressure gradient model can be obtained

$$\langle \nabla P \rangle_i = \frac{2d}{n^0} \sum_{j \neq i} \frac{P_j - \hat{P}_i}{|r_j - r_i|} (r_j - r_i) w(|r_j - r_i|), \quad (8)$$

where \hat{P}_i is the minimum pressure within the effective radius r_e . The purpose of replacing pressure P_i with \hat{P}_i is

to enforce repulsive force on all particles to stabilize the simulation.

2.2.2. Derivation of MPS. The semi-implicit scheme is adopted in MPS method. The Navier-Stokes equation is solved in two steps:

$$\left[\frac{D\mathbf{u}}{Dt}\right]^{k+1} = \left[-\frac{1}{\rho}\nabla P\right]^{k+1} + [v\nabla^2\mathbf{u}]^k + [g]k. \quad (9)$$

The superscript k represents the k th time step, and the $k+1$ represents the $(k+1)$ -th time step. The left side of Equation (9) can be divided into two parts

$$\left[\frac{D\mathbf{u}}{Dt}\right]^{k+1} = \frac{u^{k+1} - u^*}{\Delta t} + \frac{u^* - u^k}{\Delta t}. \quad (10)$$

The explicit process is conducted. The intermediate velocity is only calculated by viscosity and gravity term.

$$u^* = u^k + \Delta t [v\nabla^2\mathbf{u}]^k + \Delta t [g]k. \quad (11)$$

The intermediate position can be ascertained by

$$r^* = r^k + u^* \Delta t. \quad (12)$$

Then, the incompressible condition is enforced in the MPS method, namely, the particle number density must remain constant, as

$$n_i = n^0 \quad (13)$$

where n_i is the particle number density of the i th fluid particle.

The following Poisson equation is derived, and the pressure of particles is implicitly evaluated using this equation

$$\langle \nabla P \rangle_i^{k+1} = -\frac{\rho}{\Delta t} \frac{n_i^* - n^0}{n^0}, \quad (14)$$

where n_i^* is the temporary particle number density calculated after the explicit step. After calculating the pressure of particles, the gradient of pressure is computed by Equation (8). The velocity of the next time step is corrected by

$$u^{k+1} = u^* - \Delta t \left[-\frac{1}{\rho} \nabla P \right]^{k+1}. \quad (15)$$

The position of particles at the $(k+1)$ -th time step can be calculated

$$r^{k+1} = r^* + (u^{k+1} - u^*) \Delta t. \quad (16)$$

The Dirichlet boundary condition is enforced in the Poisson equation on the free surface. The pressure of particles is set to zero when the particle number density satisfies

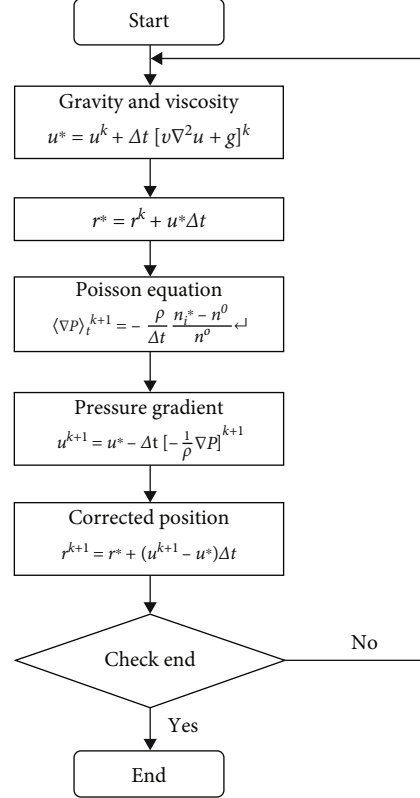


FIGURE 2: Flow chart of the MPS method.

the equation

$$n_i^* < \beta n^0, \quad (17)$$

where β is a parameter for surface detection and $\beta = 0.97$ is adopted in this study.

The solid wall boundary condition is represented by fixed boundary particles which are composed of one layer of boundary particles and several layers of dummy particles.

The flow chart of the MPS method is shown in Figure 2.

2.2.3. Biviscosity Section. The behavior of the mortar in the flow test was simulated using MPS numerical method. The governing equation is the momentum equation of the Bingham fluid. The non-Newtonian viscosity of a biviscosity model is used in this study. The momentum equation for the i th direction is as follows:

$$\frac{D\mathbf{u}_i}{Dt} = F_i + \frac{1}{\rho} \left\{ -\nabla P + \left(\eta + \frac{\tau_y (1 - e^{-m\sqrt{II}})}{\sqrt{II}} \right) \nabla^2 \mathbf{u}_i + 2\dot{\epsilon}_{ij} \frac{\partial (\tau_y (1 - e^{-m\sqrt{II}}) / \sqrt{II})}{\partial x_j} \right\}, \quad (18)$$

where F_i represents the body forces (N/m^3), ρ is the density of mortar (kg/m^3), P is the pressure (Pa), η is the plastic viscosity (Pa·s), τ_y is the yield value (Pa), m is the fitting

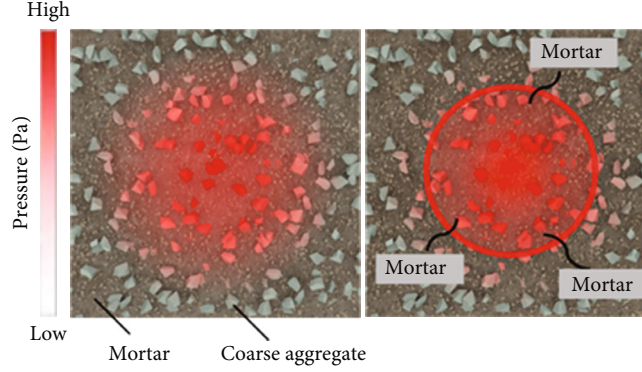


FIGURE 3: Conceptual diagram of the segregation model.

index [6], $\dot{\epsilon}_{ij}$ is the strain rate, and $\sqrt{\Pi} = \sqrt{2\dot{\epsilon}_{ij}\dot{\epsilon}_{ij}}$.

$$\dot{\epsilon}_{ij} = \frac{1}{2} \left[(\nabla u) + (\nabla u)^T \right]. \quad (19)$$

Velocity gradient of i th particle at time level k is calculated using the following gradient model

$$\langle \nabla u \rangle_i^k = \frac{d}{n^0} \sum_{j \neq i} \frac{(\mathbf{u}_j^k - \mathbf{u}_i^k)(\mathbf{r}_j^k - \mathbf{r}_i^k)}{|\mathbf{r}_j^k - \mathbf{r}_i^k|^2} \mathbf{w}(|\mathbf{r}_j^k - \mathbf{r}_i^k|), \quad (20)$$

where d is the number of space dimensions.

The viscosity coefficient is calculated between the particles i and j and average of particle i and particle j .

$$\mu_{ij} = \eta + \frac{\tau_y(1 - e^{-m\sqrt{\Pi}})}{\sqrt{\Pi}}, \quad (21)$$

$$\nu_{ij} = \frac{\mu_i + \mu_j}{2\rho}.$$

When calculating viscous items after calculating the viscous coefficient, the formulas for viscous terms are discretized using the Laplacian model as

$$u_i^* = u_i^k + \Delta t \frac{2d}{\lambda n^0} \sum_{j \neq i} \nu_{ij}^k (u_j^* - u_i^*) \mathbf{w}(|\mathbf{r}_j^* - \mathbf{r}_i^*|). \quad (22)$$

2.2.4. Segregation Section. According to the model of the previous studies proposed [33–37], segregation of material occurred because the pressure force from the difference of fresh concrete caused the mortar flows from a high-pressure area to low pressure area is used to simulate in this paper as shown as Figure 3.

$$M_i^{t+\Delta t} = M_i^t + \left(\alpha \times \frac{\sum_{j \neq i} (|P_j - P_i|) \mathbf{w}(|\mathbf{r}_j - \mathbf{r}_i|)}{\sum_{j \neq i} \mathbf{w}(|\mathbf{r}_j - \mathbf{r}_i|)} \times M_i^t \right) \times \Delta t (P_j > P_i),$$

$$M_i^{t+\Delta t} = M_i^t - \left(\alpha \times \frac{\sum_{j \neq i} (|P_j - P_i|) \mathbf{w}(|\mathbf{r}_j - \mathbf{r}_i|)}{\sum_{j \neq i} \mathbf{w}(|\mathbf{r}_j - \mathbf{r}_i|)} \times M_i^t \right) \times \Delta t (P_j < P_i), \quad (23)$$

where t is the time, M_i^t is the mix-proportion of point i , and $M_i^{t+\Delta t}$ is the proportion of mortar. α is the material segregation resistance coefficient, which is based on the change of the rheological constant assumed by this study.

The maximum and minimum of mix-proportion need to be set. The maximum of mix-proportion was set as 0.99, and minimum of mix-proportion was set as (1 ~ solid content in aggregate/100) in this paper. The mortar no longer flows into central area when the mix-proportion of point i reaches the maximum value, and the mortar will no longer flows out when the mix-proportion of point i reaches the minimum.

3. Experimental Results

The plastic viscosity coefficient reflects the flow properties of concrete. Generally, the higher the plastic viscosity, the slower the mortar flow. As listed in Table 2, the plastic viscosity for three kinds of mix proportions of grouting mortar was 2.14, 5.00, and 2.82 Pa·s, the mortar flow value within 5 seconds recorded by the camera was 245, 195, and 226 mm, respectively. The segregation resistance index γ and segregation resistance coefficient α was described as Equations (24) and (25). The relationship between flow value and time with different plastic viscosity of minislump tests was shown in Figure 4. At the same time before the flow stops, with the increase of plastic viscosity, the flow distance of grouting mortar becomes shorter. The flow time with different plastic viscosity at the same distance and the flow velocity of mortar also increases with the decrease of plastic viscosity, which is a negative correlation trend. It also directly shows that plastic viscosity is an important factor affecting the flow velocity of a cement-based material.

4. Numerical Results and Discussions

4.1. The Effects of Viscosity Coefficient on Flow Value. The purpose of slump flow simulation is to verify the implementation of the Bingham model for non-Newtonian rheology. The numerical model has a total number of particles of 121,107. The density of the fluid is 2133 kg/m³, 2156 kg/m³, and 2140 kg/m³. The rheological parameters (plastic viscosity and yield stress) of the sample were measured by viscometer as listed in Table 2. The

TABLE 2: Measured data of minislump test.

No	ρ (kg/m ³)	η_p (Pa·s)	τ_0 (Pa)	Flow* (mm)	γ	α
1	2133	2.14	22.6	245	1.23	6.1×10^{-4}
2	2156	5.00	35.18	195	1.57	7.9×10^{-4}
3	2140	2.82	26.75	226	1.32	6.6×10^{-4}

*Flow value of minislump test in 5 s (flow pattern of mortar was recorded by the camera during the test).

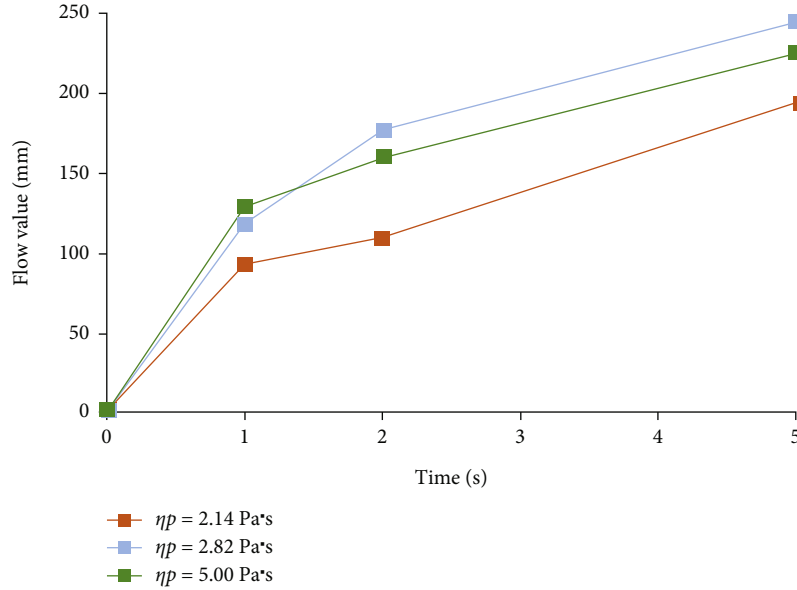


FIGURE 4: Relationship between flow value and time with different plastic viscosity.

computational time step is 0.00002 seconds, and the total computational time is 5.0 seconds.

Figure 5 shows the numerical simulation of the minislump flow process by using the modified MPS method when the plastic viscosity is 2.14 Pa·s. As illustrated in this plot, the flow value presents an increasing tendency with the rise of time. The flow value at time of 0.5 s, 1.0 s, 2.0 s, and 5.0 s was 0.085, 0.120, 0.181, and 0.241 m, respectively. Figure 6 manifests the comparison of simulation and test results. It can be seen from Figure 6 that the simulated value is in good agreement with the experimental value, but in the early stage of flow, the experimental value is smaller than the simulated value. This is caused by the delay in the lifting time of the slump cone under the test state, and the numerical simulation can achieve the ideal state of the instant lifting of the slump cone.

All of the above indicate that the flow time and pattern are affected by the rheological constant.

4.2. Assessment of Segregation Section. The numerical simulation of flow is a powerful tool for understanding the rheological behavior of flow patterns. In order to verify the availability of the segregation model depending on the rheological properties and pressure, the simulation results of the

flow test are validated with the measured data. The parameters used in the calculation are shown in Table 2.

The material segregation resistance coefficient is used in this paper, which is based on the regression analysis of the material segregation resistance index and rheological constant as shown in Table 2.

$$y = 0.072\eta + 0.011\tau + 0.827, \quad (24)$$

where y is the segregation resistance index, η is the plastic viscosity, and τ is the yield value. According to this formula, it can be known that y increases with the increase of η and τ . In addition, the segregation resistance index y represents the index of the tendency of material segregation resistance in the experiment. In addition, the material factor alpha-factor used in the analysis indicates the proportion of concrete moving in unit time and the value of segregation resistance is consistent with the tendency of segregation resistance index. Therefore, the segregation resistance index y obtained by the heavy regression equation is used as the coefficient of w ($w = 5.0 \times 10^{-4}$), which is used as the material segregation resistance coefficient α (Table 2).

$$\alpha(\eta_m^p, \tau_y) = wy. \quad (25)$$

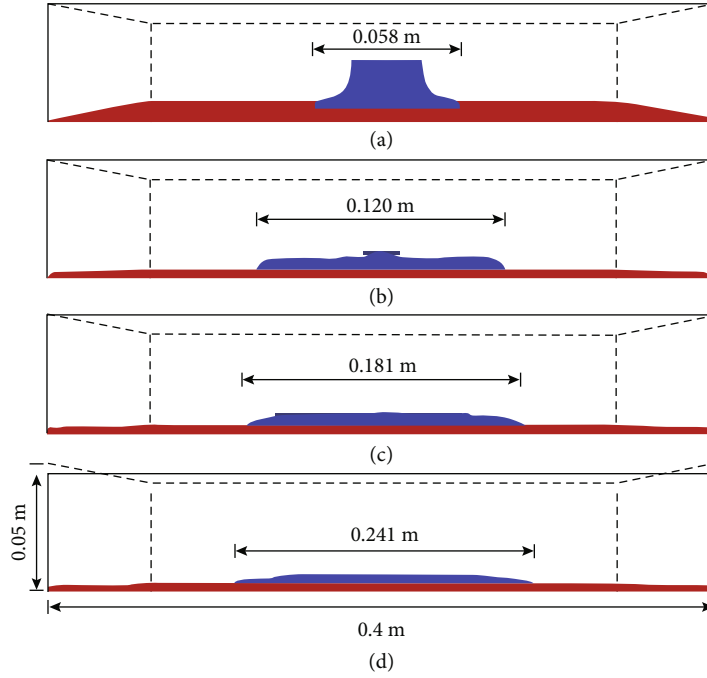


FIGURE 5: Snap shots of 3D minislump test at time of 0.5 s (a), 1.0 s (b), 2.0 s (c), and 5.0 s (d).

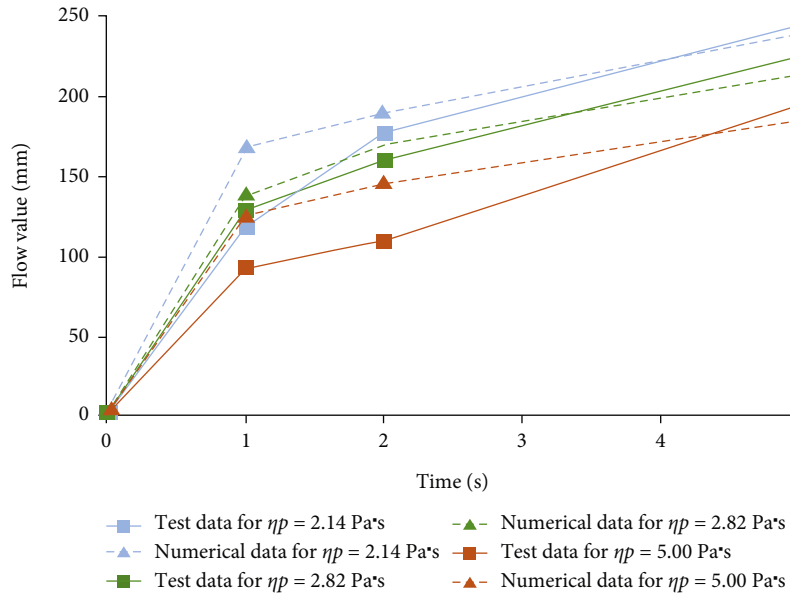


FIGURE 6: Comparison between simulation results and experiment results.

There is no unified test method for quantitative measurement of segregation of material. Therefore, from the perspective of numerical simulation, this paper verifies the feasibility of segregation section of mortar.

Numerical simulation is carried out for different test conditions, and the test flow value and simulated flow value are compared and analyzed. The errors of the two are shown in Table 3, where T_e is the test result, T_s is the simulation result, and E is the error rate. The results show that the maximum error of the simulation results is 5.1%, which shows that the segregation section established in this paper has a

TABLE 3: Accuracy of simulation.

No	(T_e/s)	(T_s^*/s)	$(E_1/\%)$	(T_s^{**}/s)	$(E_2/\%)$
1	245	233	5.0	240	2.0
2	195	179	8.2	185	5.1
3	226	211	6.6	215	4.9

T_s^*/s : Simulation result by modified MPS method without segregation section. T_s^{**}/s : Simulation result by modified MPS method with segregation section.

certain accuracy and can provide a reference basis for the flow state of mortar and concrete described by the Bingham rheological model.

5. Conclusions

Based on the results obtained in the experiment and the numerical simulation, it is clear that plastic viscosity and yield stress have the great influence on the flow time of mortar, and with the increase of plastic viscosity, the time to flow to the specified area also increases.

A good agreement between numerical and experimental data was found in the comparison of the final shape of the sample. It can be known that the modified MPS method in this paper is feasible for the flow simulation of grouting mortar and has high accuracy. The investigated results indicate that the modified MPS method by setting reasonable particle spacing can simulate and predict the flow process of non-Newtonian fluid with a free surface. The effectiveness of the segregation section depending on the rheological properties and pressure proposed in this paper was verified. Through the comparison between the numerical simulation and the experimental results, it is found that the simulation accuracy was improved from 91.8% to 94.9%, which showed that the segregation section was suitable for the simulation of the grouting mortar.

Data Availability

All data, models, and code generated or used during the study are available from the corresponding author by request.

Disclosure

A preprint has previously been published [38].

Conflicts of Interest

The authors declare that they have no conflicts of interest.

Authors' Contributions

Ailifeila Aierken contributed to the methodology and writing-original draft. Shilin Luo contributed to the conceptualization and revision. Jianqing Jiang contributed to the data curation and language editing. Linlin Chong and Jin Chang contributed to the algorithm analysis. Rui Zhang and Xiangchao Zhang contributed to the software and validation.

Acknowledgments

This work was supported by the Hunan Provincial Natural Science Foundation (Nos 22021JJ40632, 2021JJ30758 and 2022JJ40521), Scientific Research Project from the Education Department of Hunan Province (Nos 21C0740, 21C0753, and 21B0773), and Changsha Municipal Natural Science Foundation (Nos kq2007089, kq2202065, and kq2202063).

References

- [1] J. Wu and C. Shu, "An improved immersed boundary-lattice Boltzmann method for simulating three-dimensional incompressible flows," *Journal of Computational Physics*, vol. 229, no. 13, pp. 5022–5042, 2010.
- [2] O. Švec, J. Skoček, H. Stang, M. R. Geiker, and N. Roussel, "Free surface flow of a suspension of rigid particles in a non-Newtonian fluid: a lattice Boltzmann approach," *Journal of Non-Newtonian Fluid Mechanics*, vol. 179–180, pp. 32–42, 2012.
- [3] F. P. T. Baaijens, "A fictitious domain/mortar element method for fluid-structure interaction," *International Journal for Numerical Methods in Fluids*, vol. 35, no. 7, pp. 743–761, 2001.
- [4] E. Secrieru, J. Khodor, C. Schröfl, and V. Mechtcherine, "Formation of lubricating layer and flow type during pumping of cement-based materials," *Construction and Building Materials*, vol. 178, pp. 507–517, 2018.
- [5] M. Choi, C. F. Ferraris, N. S. Martys, D. Lootens, V. K. Bui, and H. R. T. Hamilton, "Metrology needs for predicting concrete pumpability," *Advances in Materials Science and Engineering*, vol. 2015, 10 pages, 2015.
- [6] M. S. Choi, Y. J. Kim, and S. H. Kwon, "Prediction on pipe flow of pumped concrete based on shear-induced particle migration," *Cement and Concrete Research*, vol. 52, pp. 216–224, 2013.
- [7] G. R. Liu and M. B. Liu, *Smoothed Particle Hydrodynamics*, World Scientific Publishing Co, Pte Ltd, 2003.
- [8] Z. Li, Z. Xu, and R. Yoshioka, *Flow Simulation of Fresh Concrete Using SPH Method with Consideration of Geometry of Particles*, in: *Sixth Int. Conf. Constr. Mater*, Fukuoka, Japan, 2020.
- [9] G. Cao, Z. Li, and Z. Xu, "A SPH simulation method for opening flow of fresh concrete considering boundary restraint," *Construction and Building Materials*, vol. 198, pp. 379–389, 2019.
- [10] W. S. Alyhya, S. Kulasegaram, and B. L. Karihaloo, "Simulation of the flow of self-compacting concrete in the V-funnel by SPH," *Cement and Concrete Research*, vol. 100, pp. 47–59, 2017.
- [11] G. Cao and Z. Li, "Numerical flow simulation of fresh concrete with viscous granular material model and smoothed particle hydrodynamics," *Cement and Concrete Research*, vol. 100, pp. 263–274, 2017.
- [12] M. S. Abo Dhaheer, S. Kulasegaram, and B. L. Karihaloo, "Simulation of self-compacting concrete flow in the J-ring test using smoothed particle hydrodynamics (SPH)," *Cement and Concrete Research*, vol. 89, pp. 27–34, 2016.
- [13] S. Koshizuka and Y. Oka, "Moving-particle semi-implicit method for fragmentation of incompressible fluid," *Nuclear Science and Engineering*, vol. 123, no. 3, pp. 421–434, 1996.
- [14] Y. Shimizu, H. Gotoh, and A. Khayyer, "An MPS-based particle method for simulation of multiphase flows characterized by high density ratios by incorporation of space potential particle concept," *Computers & Mathematics with Applications*, vol. 76, no. 5, pp. 1108–1129, 2018.
- [15] Z. Xu, Z. Li, G. Cao, and F. Jiang, "Comparison of SPH and MPS methods for numerical flow simulations of fresh mortar," *Proceeding of the Japan concrete institute*, vol. 41, pp. 1127–1132, 2019.
- [16] Z. Xu, Z. Li, and F. Jiang, "The applicability of SPH and MPS methods to numerical flow simulation of fresh cementitious

- materials,” *Construction and Building Materials*, vol. 274, p. 121736, 2021.
- [17] J. Li, L. Tian, L. Qiu, and H. Yu, “Numerical simulation of self-compacting concrete flow based on MPS method,” *Journal of Building Materials*, vol. 23, no. 2, pp. 309–316, 2020.
- [18] L. I. Jing-jun, T. I. A. N. Lei, and Q. I. U. Liu-chao, “Numerical simulation for the filling of RFC based on MPS method,” *Journal of Building Materials*, vol. 23, no. 6, pp. 1357–1365, 2020.
- [19] Y. Zhao, C. Zhang, Y. Wang, and H. Lin, “Shear-related roughness classification and strength model of natural rock joint based on fuzzy comprehensive evaluation,” *International Journal of Rock Mechanics and Mining Sciences*, vol. 137, article 104550, 2021.
- [20] Y. Zhao, Q. Liu, C. Zhang, J. Liao, H. Lin, and Y. Wang, “Coupled seepage-damage effect in fractured rock masses: model development and a case study,” *International Journal of Rock Mechanics and Mining Sciences*, vol. 144, article 104822, 2021.
- [21] D. Sun, H. Wen, J. Xu, Y. Zhang, D. Wang, and J. Zhang, “Improving geospatial agreement by hybrid optimization in logistic regression-based landslide susceptibility modelling,” *Frontiers in Earth Science*, vol. 9, no. 8, pp. 117–129, 2021.
- [22] Y. C. Jin, K. Guo, Y. C. Tai, and C. H. Lu, “Laboratory and numerical study of the flow field of subaqueous block sliding on a slope,” *Ocean Engineering*, vol. 124, no. 15, pp. 371–383, 2016.
- [23] E. Harada, H. Ikari, T. Tazaki, and H. Gotoh, “Numerical simulation for coastal morphodynamics using DEM-MPS method,” *Applied Ocean research*, vol. 117, article 102905, 2021.
- [24] Z. Xu, Z. Li, and F. Jiang, “Numerical approach to pipe flow of fresh concrete based on MPS method,” *Cement and Concrete Research*, vol. 152, article 106679, 2022.
- [25] P. Yu, Y. H. Duan, Q. X. Fan, and S. W. Tang, “Improved MPS model for concrete creep under variable humidity and temperature,” *Construction and Building Materials*, vol. 243, article 118183, 2020.
- [26] Y. Pan, H. Wang, Y. Zhao, Q. Liu, and S. Luo, “Numerical analysis of the mud inflow model of fractured rock mass based on particle flow,” *Geofluids*, vol. 2021, Article ID 5599748, 16 pages, 2021.
- [27] Y. Z. Q. Liu, J. Lian, Y. Wang, and L. Tang, “Theoretical and numerical models of rock wing crack subjected to hydraulic pressure and far-field stresses,” *Arabian Journal of Geosciences*, vol. 13, no. 18, p. 926, 2020.
- [28] J. Liao, Y. Zhao, L. Tang, and Q. Liu, “Experimental studies on cracking and local strain behaviors of rock-like materials with a single hole before and after reinforcement under biaxial compression,” *Geofluids*, vol. 2021, Article ID 8812006, 15 pages, 2021.
- [29] L. Tang, Y. Zhao, J. Liao, and Q. Liu, “Creep experimental study of rocks containing weak interlayer under multi-level loading and unloading cycles,” *Frontiers in Earth Science*, vol. 8, article 519461, 2020.
- [30] Y. Zhao, Y. Wang, W. Wang, W. Wan, and J. Tang, “Modeling of non-linear rheological behavior of hard rock using triaxial rheological experiment,” *International Journal of Rock Mechanics and Mining Sciences*, vol. 93, pp. 66–75, 2017.
- [31] H. Lin, D. Lei, C. Zhang, Y. Wang, and Y. Zhao, “Deterioration of non-persistent rock joints: a focus on impact of freeze-thaw cycles,” *International Journal of Rock Mechanics & Mining Sciences*, vol. 135, article 104515, 2020.
- [32] F. Miao, Y. Wu, Á. Török, L. Li, and Y. Xue, “Centrifugal model test on a riverine landslide in the Three Gorges Reservoir induced by rainfall and water level fluctuation,” *Geoscience Frontiers*, vol. 13, no. 3, p. 101378, 2022.
- [33] S. Hirano, Y. Yamada, H. Nishi, and K. Sakihara, “rheological constants measurement of mortar that fluidity is evaluated by slump and analysis of slump and slump flow of mortar by MPS method,” *Journal of Structural and Construction Engineering (Transactions of AIJ)*, vol. 85, no. 774, pp. 993–1003, 2020.
- [34] Y. Higashifunamichi and Y. Yamada, “Study on the rheological constants estimation method of cement paste by flow test,” *Journal of Structural and Construction Engineering (Transactions of AIJ)*, vol. 86, no. 784, pp. 860–870, 2021.
- [35] P. Xie, H. Wen, S. Ma et al., “The bearing capacity analysis of limestone strata roof containing a shallow-buried cylinder Karst cave,” *Mechanics of Advanced Materials and Structures*, vol. 12, no. 33, pp. 1–8, 2021.
- [36] Y. Yamada, Y. Uehara, K. Sakihara, and S. Urano, “Slump flow simulation of high fluidity concrete by MPS method,” *Journal of Structural and Construction Engineering (Transactions of AIJ)*, vol. 85, no. 771, pp. 663–672, 2020.
- [37] Z. Xu and Z. Li, “Numerical method for predicting flow and segregation behaviors of fresh concrete,” *Cement and Concrete Composites*, vol. 123, p. 104150, 2021.
- [38] A. Aierken, *Study on Flow Properties and Segregation-resistance Performance on Filling Behavior of Grout Mortar*, [Ph.D. thesis], Tokyo Metropolitan University, Tokyo, 2018.